Jander, W., "Reaktionen im festen Zustande bei hoheren Temperaturen," *Z. Anorg. Allgem. Chem.*, **163**, 1 (1927).
Luss, D., "On the Pseudo Steady State Approximation for Gas Solid Reactions," *Can. J. Chem. Eng.*, **46**, 154 (1968).
Petersen, E. E., "Reaction of Porous Solids," *AIChE J.*, **3**, 442 (1957).
Ramachandran, P. A., and J. M. Smith, "Effect of Sintering and Porosity Changes on Rates of Gas-Solid Reactions," *Chem. Eng. J.*, **14**, 137 (1977a).
Ramachandran, P. A., and J. M. Smith, "A Single-Pore Model for Gas-Solid Non-Catalytic Reactions," *AIChE J.*, **23**, 353 (1977b).
Satterfield, C. N., *Mass Transfer in Heterogeneous Catalysis*, M.I.T. Press, Cambridge, MA (1970).
Smith, J. M., *Chemical Engineering Kinetics*, McGraw Hill, New York (1970).
Szekely, J., and J. W. Evans, "A Structural Model for Gas-Solid Reactions with a Moving Boundary," *Chem. Eng. Sci.*, **25**, 1091 (1970).
Szekely, J., J. W. Evans, and H. Y. Sohn, *Gas-Solid Reactions*, Academic Press, London (1976).

Manuscript received October 23, 1981; revision received April 12, and accepted April 26, 1982.

Discrete Cell Model of Pore-Mouth Poisoning of Fixed-Bed Reactors

Catalyst deactivation in an isothermal fixed-bed reactor under pore-mouth poisoning conditions is investigated theoretically using a discrete mixing cell model. Two fundamental relationships which characterize the poisoning process in the reactor are identified and incorporated into the model to develop a simple graphical procedure for a quick, general insight into the problem. This graphical method is extended to design pellet impregnation profiles along the reactor which would give nondeteriorating reactor performance up to a given time. The effects of various system parameters on the lifetime and conversion performance of the reactor are also examined analytically, graphically and numerically.

B. K. CHO and L. L. HEGEDUS

General Motors Research Laboratories
Warren, MI 48090
and
RUTHERFORD ARIS
University of Minnesota
Minneapolis, MN 55455

SCOPE

Deactivation of catalyst pellets due to pore-mouth poisoning and the associated performance degradation of fixed-bed catalytic reactors have been extensively treated by numerous investigators for the past two decades. However, all previous approaches were confined to continuum models in which the poisoning process is described by coupled partial differential equations.

The main purpose of this work is to investigate the poison accumulation and deactivation process in a fixed-bed catalytic reactor under pore-mouth poisoning conditions through the use of a discrete mixing cell model.

It is demonstrated that a useful insight into the reactor behavior can be readily obtained without solving the partial differential equations inherent to the continuum model, and furthermore the discrete model equations can be solved through a simple graphical procedure which plays a role similar to the McCabe-Thiele method in distillation column design. This graphical procedure is then employed to the optimum design of a poison-resistant catalytic reactor.

The effect of gas-phase dispersion on the reactor's lifetime is examined for various types of noble metal impregnation patterns in the catalyst pellets. The effects of noble metal loadings, the impregnation pattern, and the effective diffusivity of catalyst pellets as well as the effect of gas-phase mixing on the conversion performance of the reactor are studied.

CONCLUSIONS AND SIGNIFICANCE

The discrete mixing cell model developed in this paper demonstrates a clear computational advantage over the traditional continuum model for simulating the pore-mouth poisoning process in a fixed-bed catalytic reactor.

Due to its discrete nature, this model allows one to determine the poison profile, the lifetime, and the conversion performance of a fixed-bed reactor through a simple graphical procedure. This graphical procedure can be readily extended to investigate the optimum noble metal impregnation profiles along the reactor which would give non-deteriorating reactor performance throughout a given reactor operating time.

Mixing characteristics in the gas phase do not influence the reactor lifetime when catalyst pellets are uniformly or core impregnated. For subsurface or peripherally impregnated catalysts, however, the reactor lifetime becomes shorter with increased mixing in the gas phase.

For a first-order main reaction under pore-mouth poisoning, a plug-flow reactor gives higher conversion than a well-mixed reactor for shorter reactor operating times, while a well-mixed reactor gives higher conversion for longer operating times. There is a point in time when the two reactors give equivalent conversion performance.

INTRODUCTION

When a fixed-bed catalytic reactor operates under the condition that the reaction rate of the poison precursor (e.g., impurity in the feed) with the catalyst support or the catalytic sites is much faster than the poison precursor's diffusion rate through the pores, the overall poisoning process is limited by the rate of poison precursor diffusion across the poisoned shell of the catalyst. A quantitative understanding of such pore-mouth poisoning is of considerable

L. L. Hegedus is presently with W. R. Grace & Co., Columbia, MD 21044.

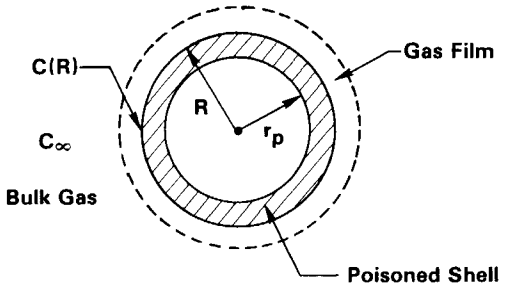

Figure 1. Cross section of a catalyst pellet under pore-mouth poisoning.

practical importance; one typical example is the phosphorus poisoning of alumina-supported automobile exhaust catalysts (Hegedus and Summers, 1977; Hegedus and Baron, 1978). In this poisoning process, the poison precursor penetrates the catalyst pellet in the form of a reasonably sharp front, reducing the effectiveness of the catalyst.

The deactivation of a single catalyst pellet under pore-mouth poisoning conditions has been discussed, e.g., by Carberry and Gorring (1966), Murakami et al. (1968), Valdman et al. (1976), Becker and Wei (1977), and Varghese and Wolf (1980). The problem of poison accumulation in a fixed-bed catalytic reactor has also been the subject of numerous investigations. For example, modeling of the time-dependent activity of a fixed-bed reactor under conditions of poisoning by coke formation or irreversible adsorption of a feed component has received considerable attention in the past two decades (Froment and Bischoff, 1961; Olson, 1968; Wheeler and Robell, 1969; Haynes, 1970; Moriyama, 1971; DeLancey, 1973; Hegedus and Baron, 1978). All of the previous approaches were based on plug-flow continuum models which require the solving of coupled first-order partial differential equations.

In this work, however, we simulate the performance of a fixed-bed catalytic reactor during pore-mouth poisoning by a cascade of discrete mixing cells, instead of the traditional continuum model. As we shall see, by this approach the solution to the problem can be obtained by a simple graphical procedure, rather than by numerically solving the partial differential equations.

The influence of poisoning on the conversion performance of the reactor will be examined for a first-order main reaction.

MATHEMATICAL FORMULATION

Poison Accumulation in a Single Catalyst Pellet

A schematic diagram of a spherical catalyst pellet under pore-mouth poisoning conditions is shown in Figure 1. The outer layer of the catalyst pellet (cross-hatched in Figure 1) is represented by a poisoned shell through which the reactants must diffuse before they can find any available catalytic sites. The poison penetration in a single catalyst pellet through pore-mouth type poisoning has been analyzed previously (e.g., Carberry and Gorring, 1966; Olson, 1968), and only the relevant equations will be presented here.

We consider here the case where nonselective poisoning of the catalyst pellet by a pore-mouth mechanism due to an impurity in the feed occurs independently of the main reaction. We also consider the interface between the active inner core and the poisoned outer shell (i.e., $r = r_p$ in Figure 1) to be stationary at a given instant of time; thus a steady-state diffusion equation for the poison precursor can be solved to find its intrapellet concentration profile at each time.

With the pseudosteady-state hypothesis, the diffusion equation for the poison precursor becomes

$$D_e \frac{1}{r^2}\frac{\partial}{\partial r}\left(r^2 \frac{\partial c}{\partial r}\right) = 0, \tag{1}$$

with the boundary conditions

$$k_m[c_\infty - c(R)] = D_e \frac{\partial c}{\partial r}(R) \text{ and} \tag{1a}$$

$$c(r_p) = 0. \tag{1b}$$

The boundary condition 1b follows directly from the assumption that the reaction between the poison precursor and the catalyst support (and the active catalytic sites) is infinitely fast. Solving Eq. 1 together with Eqs. 1a and 1b, we obtain the rate of poison precursor diffusion into a single pellet

$$J(t) = 4\pi R D_e c_R \left\{\frac{\xi(t)}{1-(1-\beta)\xi(t)}\right\}\Psi(t), \tag{2}$$

where

$$\beta = D_e/Rk_m, \qquad \xi = r_p/R, \qquad \Psi = c_\infty/c_R.$$

Here c_R is a reference concentration which will be appropriately chosen later.

We define λ, the saturation concentration of the poison precursor in the catalyst (mol/cm^3 pellet), as

$$\lambda \equiv 3\int_0^\infty J(t)dt/4\pi R^3. \tag{3}$$

Then the average poison concentration in the pellet at time t is given by

$$\lambda(1-\xi(t)^3) = 3\int_0^t J(t)dt/4\pi R^3, \tag{4}$$

if the catalyst is initially poison-free.

Introducing the dimensionless time

$$\tau = 6D_e c_R t/\lambda R^2,$$

Equation 4 can be transformed to

$$\frac{df}{d\tau} = \Psi(\tau) \tag{5}$$

or, equivalently, to

$$f(\xi(\tau)) = \int_0^\tau \Psi(\tau')d\tau', \tag{6}$$

where

$$f(\xi(\tau)) = 3(1-\xi(\tau)^2) - 2(1-\beta)(1-\xi(\tau)^3). \tag{7}$$

It follows directly from Eqs. 6 and 7 that the time required for the poison front to reach the pellet center, τ_c, can be obtained from

$$1 + 2\beta = \int_0^{\tau_c} \Psi(\tau)d\tau. \tag{8}$$

The function $f(\xi)$ (Eq. 6) represents the total "exposure" of a catalyst pellet to the poison precursor over a period 0 to τ.

For the case of constant gas-phase poison precursor concentration, the reference concentration c_R can be conveniently taken to be c_∞ and thus $\Psi = 1$. In this case, Eq. 6 can be reduced to the following expression for the radial location of the poison front at time τ (Bischoff, 1963, Carberry and Gorring, 1966; Levenspiel, 1972):

$$\tau = f(\xi(\tau)). \tag{9}$$

Mixing Cell Reactor Model for Poison Propagation

In this work, a fixed-bed reactor is simulated by a cascade of mixing cells, Figure 2. The appropriate number of mixing cells, N, depends, in general, on the degree of gas-phase dispersion in the reactor. Detailed discussions of the criterion for a proper choice of N can be found elsewhere (Levenspiel, 1973; Mecklenburgh and Hartland, 1975). We assume that the catalyst pellets in each mixing cell are stationary and are exposed to a uniform bulk gas phase concentration under isothermal conditions.

The poison precursor's mass balance for the i-th cell is

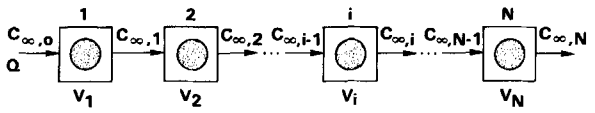

Figure 2. A mixing cell model of a fixed-bed reactor.

TABLE 1. STANDARD SET OF PARAMETER VALUES

Catalyst Pellet

0.048 wt% Pt (70% dispersion)

ρ_p = 0.783 g/cm³ pellet

S_g = 882 cm² Pt/g pellet

R = 0.16 cm

D_e = 0.0471 cm²/s, $D_{e,A}$ = 0.0724 cm²/s } (at 773 K, 1 atm)

k = 1.299×10^3 cm³/(s · cm² Pt)

Φ_A = 563

Converter

Volume = 4,261 cm³ (type 260)

Frontal Area = 838.7 cm²

Depth = 5.08 cm

ϵ = 0.36

N = 16

Exhaust Gas

Feed concentration { Poison precursor = 0.045 ppm by vol; Oxygen = 1.5 vol%

P = 1 atm

T = 500°C (= 773 K)

Q = 9.213×10^4 cm³/s (at 773 K, 1 atm)

k_m = 16.5 cm/s

$k_{m,A}$ = 22.6 cm/s

$$\epsilon V_i \frac{dc_{\infty,i}}{dt} = Q(c_{\infty,i-1} - c_{\infty,i}) - \frac{3(1-\epsilon)V_i}{4\pi R^3} J_i(t). \quad (10)$$

Equations 2 and 10 can be combined into the dimensionless equation

$$\Theta \frac{d\Psi_i}{d\tau} = \Psi_{i-1} - \Psi_i - \mu_i \left\{ \frac{\xi_i}{1-(1-\beta)\xi_i} \right\} \Psi_i, \quad (11)$$

with

$$\Theta = 6\epsilon V_i D_e c_R / \lambda Q R^2 \text{ and} \quad (12)$$

$$\mu_i = 3(1-\epsilon)V_i D_e / Q R^2. \quad (13)$$

For the purpose of our analysis we choose $c_{\infty,0}$, the concentration of the poison precursor in the reactor feedstream, as our reference concentration so that

$$\Psi_0 = 1. \quad (14)$$

For most gas-solid systems, the ratio $c_{\infty,0}/\lambda$ is very small (Bischoff, 1963; Carberry and Gorring, 1966); for example, it varies between 10^{-9} and 10^{-5} for typical automobile catalytic converter operating conditions (Hegedus and Baron, 1978). Therefore, under the conditions considered in this study (Table 1), Θ is negligibly small and the pseudosteady-state hypothesis can be safely invoked for Eq. 11 (i.e., $\Theta d\Psi_i/d\tau = 0$) to yield the relationship

$$\Psi_i = \Psi_{i-1} G_i, \quad (15)$$

where G_i, the transfer function of the i-th cell, relates the gas phase poison concentration of the $(i-1)$th cell to that of the i-th cell and is given by

$$G_i = \frac{1-(1-\beta)\xi_i}{1-(1-\beta)\xi_i + \mu_i \xi_i}. \quad (16)$$

Combining Eqs. 5, 15 and 16 yields

$$f(\xi_i) + 2\mu_i(1-\xi_i^3) = \int_0^\tau \Psi_{i-1}(\tau')d\tau' \quad (17)$$

or

$$h(\xi_i) = f(\xi_{i-1}), \quad (18)$$

where $h(\xi_i)$ is defined as

TABLE 2. CATALYST IMPREGNATION PATTERNS CONSIDERED

Types	Impregnation Radii	Geometric Configuration
Uniform	$r_a = 0, r_b = R$	
Core	$r_a = 0, 0 < r_b < R$	
Peripheral	$0 < r_a < R, r_b = R$	
Subsurface	$0 < r_a < r_b < R$	

r_a = inner radius of impregnated zone
r_b = outer radius of impregnated zone

$$h(\xi_i) \equiv f(\xi_i) + 2\mu_i(1-\xi_i^3). \quad (19)$$

It is obvious from Eqs. 6 and 18 that the functions $f(\xi_i)$ and $h(\xi_i)$ are directly proportional to the total amount of the poison precursor leaving the i-th cell and the $(i-1)$th cell, respectively. Then Eq. 19 simply states that the difference in throughputs between two adjacent cells (i-th and $(i-1)$th) determines the degree of poison saturation of the pellets in the i-th cell.

The relationship given by Eq. 18 allows one to predict the poison penetration depth in the i-th cell from the known properties of the $(i-1)$th cell. As will be illustrated later, this can be conveniently accomplished by a step-by-step graphical procedure in the plane of (h,f) vs. ξ.

For convenience we define the complete poisoning time of the i-th cell in the N-cell reactor $\tau_{c,i}^N$ as the time required for the front of the poisoned shell to reach the center of the pellet. However, for simplicity of notation, $\tau_{c,i}$ will be used instead of $\tau_{c,i}^N$ unless clarity requires the use of the full notation.

It follows from Eqs. 7 and 17 that the complete poisoning time for the pellets in the i-th cell should satisfy

$$\int_0^{\tau_{c,i}} \Psi_{i-1} d\tau = 1 + 2\beta + 2\mu_i. \quad (20)$$

By dividing Eq. 20 by D_e, we can see that the internal $(1/D_e)$ and the external $(1/k_m)$ transport resistances have additive effects in prolonging catalyst lifetime (e.g., Hegedus, 1974).

POISON PROPAGATION AND REACTOR LIFETIME

How poison propagation occurs along the reactor and how it affects the lifetime of the whole reactor is of considerable practical interest.

Table 2 shows four different catalyst impregnation patterns considered in our analysis. In the following discussion, we define reactor lifetime as the time required for the front of the poisoned shell (r_p in Figure 1) to reach the inner radius of the impregnated active zone (r_a in Table 2) in the last cell of the reactor.

Uniformly or Core Impregnated Pellets

Reactor Lifetime. Because $\tau_{c,i} > \tau_{c,i-1}$ for any given N, it is convenient to rewrite Eq. 20 as

$$1 + 2\beta + 2\mu_i = \int_0^{\tau_{c,i-1}} \Psi_{i-1} d\tau + \int_{\tau_{c,i-1}}^{\tau_{c,i}} \Psi_{i-1} d\tau. \quad (21)$$

From Eq. 8, the first term on the r.h.s. of Eq. 21 is equal to $(1 + 2\beta)$. Also, the integrand on the second term is unity for $\tau_{c,i-1} < \tau < \tau_{c,i}$, because all the cells up to the $(i-1)$th cell have already been completely poisoned. Thus,

$$\tau_{c,i} - \tau_{c,i-1} = 2\mu_i. \quad (22)$$

Note that Eq. 22 is valid for $i \geq 2$. For the first cell (i.e., $i = 1$), Eq. 20 gives

$$\tau_{c,1} = 1 + 2\beta + 2\mu_i. \quad (23)$$

Summation of Eq. 22 from $i = 2$ to $i = N$, with the aid of Eq. 23, gives the lifetime of a catalytic reactor with N mixing cells,

$$\tau_{c,N} = 1 + 2\beta + 2\sum_{i=1}^{N} \mu_i, \quad (24)$$

where

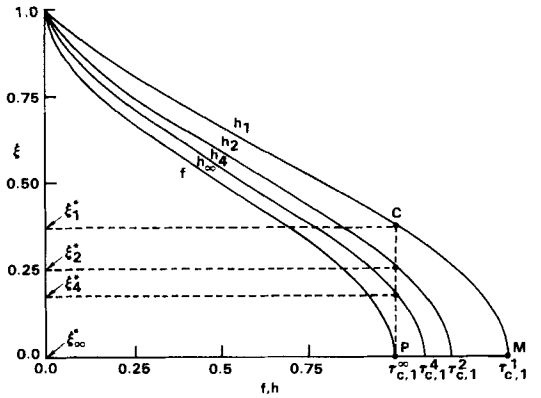

Figure 3. Typical forms of f-curve and h-curve ($\beta = 0$, $\mu = 0.1634$).

$$\mu = \sum_{i=1}^{N} \mu_i = 3(1-\epsilon)VD_e/QR^2. \tag{25}$$

It is interesting to note that $\tau_{c,N}$ is independent of N; that is, the lifetime of a catalytic reactor under pore-mouth poisoning conditions is not influenced by the gas-phase mixing characteristics when the pellets are uniformly or core impregnated. In Figure 3, $f(\xi)$ and $h_N(\xi)$ are plotted for reactors having the same volume, but different degrees of gas-phase mixing. (The curve $h_N(\xi)$ corresponds to a reactor with N mixing cells.) Notice that the curve $f(\xi)$ is independent of N, and as N increases the h-curve uniformly approaches the f-curve, eventually coinciding with the f-curve for the case of a plug-flow reactor (i.e., $h_\infty = f$).

For the first cell of the N-cell reactor, Eq. 23 can also be written as

$$\tau_{c,1}^{N} = f(0) + 2\mu/N.$$

The physical meaning of the above relation can be seen in Figure 3. A well-mixed reactor is shown to be completely poisoned at $\tau = \tau_{c,1}^{1}$. For a plug-flow reactor, its inlet boundary becomes completely poisoned at $\tau = \tau_{c,1}^{\infty} = f(0)$, whereas the whole reactor is completely poisoned at $\tau = \tau_{c,1}^{1}$ (i.e., the same reactor lifetime as a well-mixed reactor). Thus, the length of the horizontal line PM represents the time required for the complete poisoning front to travel through a plug-flow reactor.

The vertical line PC gives the poison penetration depth in the first cell at time $\tau_{c,1}^{\infty}$ for various degrees of gas phase dispersion. At this time the front end of the plug-flow reactor is completely poisoned, whereas the catalyst pellets in the well-mixed reactor have a poison penetration up to ξ_1^*. The first cell of the two-cell and four-cell reactors will have poison penetrations up to ξ_2^* and ξ_4^*, respectively.

Poison Profile Along the Reactor. When none of the cells are completely poisoned ($0 \le \tau \le t_{c,1}$), Eqs. 14, 17 and 19 give the following relationships for the first cell:

$$h(\xi_1(\tau)) = \tau \quad \text{and} \tag{26}$$

$$\Psi_1 = G_1, \tag{27}$$

and also for the i-th cell ($i \ge 2$):

$$h(\xi_i(\tau)) = f(\xi_{i-1}(\tau)) \quad \text{and} \tag{28}$$

$$\Psi_i = \prod_{j=1}^{i} G_j. \tag{29}$$

Equations 26 through 29 define the operating lines of the poisoning process in the fixed-bed reactor under the condition that no cell has been completely poisoned, that is, for $0 \le \tau \le \tau_{c,1}$. These equations provide a convenient means of examining the poisoning behavior of the whole reactor through cell-by-cell stage-wise graphical construction based only on the general $h(\xi)$ and $f(\xi)$ curves.

Figure 4 illustrates the cell-by-cell construction procedure for the pore-mouth poisoning process for the case of four mixing cells.

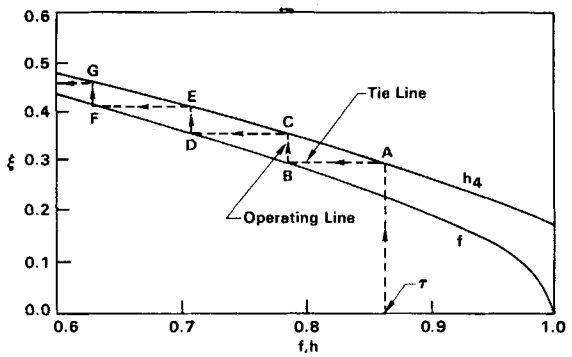

Figure 4. Graphical procedure for $0 \le \tau \le \tau_{c,1}$ ($N = 4$, $\beta = 0$, $\mu = 0.1634$).

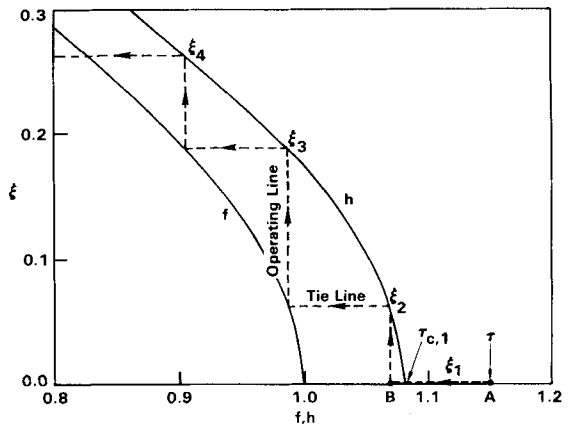

Figure 5. Graphical procedure for $\tau_{c,1} \le \tau \le \tau_{c,2}$ ($N = 4$, $\beta = 0$, $\mu = 0.1634$).

The curves $f(\xi)$ and $h(\xi)$ were generated using Eqs. 7 and 18, respectively. To calculate the poison penetration depth in each cell at a given time τ, use is made of Eq. 26 first. The vertical line anchored at τ intersects the h-curve at point A to give $h(\xi_1(\tau))$; the horizontal tie line from A intersects the f-curve at B to give $f(\xi_1(\tau))$; and another vertical operating line from B intersects the h-curve at C to give $h(\xi_2(\tau))$, and so on. The radial location of the poison front in each cell is given by the ξ values corresponding to points A, C, E, and G. Notice, however, that this graphical procedure just described can be used only when none of the cells is completely poisoned.

When some of the cells are already completely poisoned ($\tau > \tau_{c,1}$), the previous graphical procedure must be modified. To illustrate the modified graphical procedure, let us assume, without loss of generality, that all the cells up to the $(i-1)$th become completely poisoned. For $\tau_{c,i-1} < \tau < \tau_{c,i}$, then

$$\xi_{j-1} = 0, \qquad \Psi_{j-1} = 1 \qquad (j \le i). \tag{30}$$

For the i-th cell, Eq. 17 can be rewritten as

$$\begin{aligned} h(\xi_i(\tau)) &= \int_0^{\tau_{c,i-1}} \Psi_{i-1} d\tau + \int_{\tau_{c,i-1}}^{\tau} \Psi_{i-1} d\tau \\ &= f(\xi_{i-1}(\tau_{c,i-1})) + \tau - \tau_{c,i-1} \\ &= f(0) + \tau - \tau_{c,i-1} \end{aligned} \tag{31}$$

From Eqs. 7, 22 and 23, we obtain

$$\tau_{c,i} - f(0) = 2i\mu_i \qquad (i \ge 1) \tag{32}$$

and thus Eq. 31 becomes

$$h(\xi_i(\tau)) = \tau - 2(i-1)\mu_i. \tag{33}$$

For the j-th cell ($j \ge i+1$), it is obvious that we have

$$h(\xi_j(\tau)) = f(\xi_{j-1}(\tau)). \tag{34}$$

Equations 33 and 34 define the operating lines of the poisoning

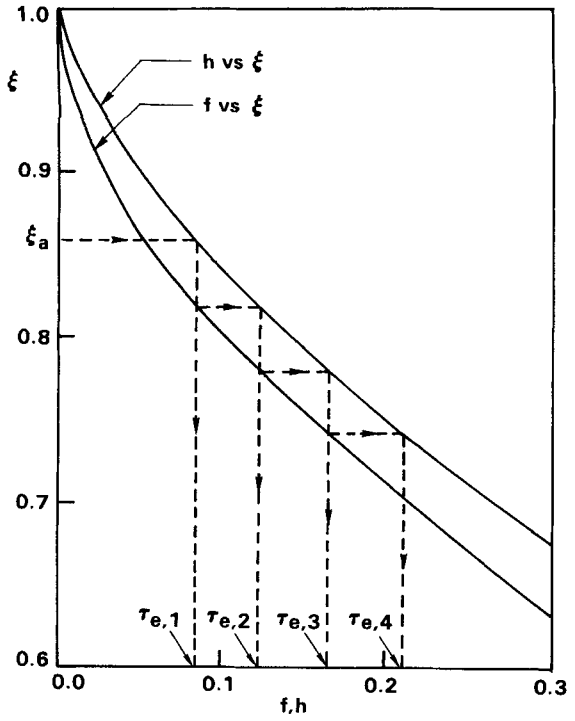

Figure 6. Effective poisoning time of a subsurface- or peripherally impregnated pellet ($N = 4, \beta = 0, \mu = 0.1634$).

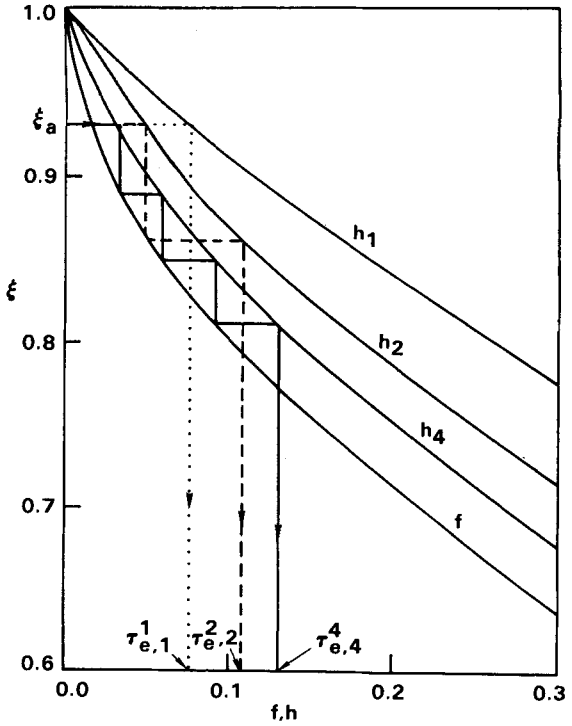

Figure 7. Effect of gas-phase mixing on the reactor's lifetime ($\beta = 0, \mu = 0.1634$).

process when all the cells up to the $(i-1)$th are already completely poisoned. Comparison of Eqs. 26 and 33 indicates that the additional term $2(i-1)\mu_i$ in Eq. 33 accounts for the presence of the completely poisoned cells.

The modified graphical procedure is illustrated in Figure 5, for the case of four cells and $\tau_{c,1} < \tau < \tau_{c,2}$. From Eq. 33 the length of the line segment BA is $2\mu_i$. Once point B is located, the poison penetration depths in the second and the following cells can be obtained by the same graphical procedure described in the previous section.

From Figure 3 and Eq. 32, it may be deduced that

$$\tau^N_{c,i} = \tau^M_{c,j} \qquad \text{if } N/M = i/j.$$

In other words, for example, the complete poisoning time of the second cell in the four-cell reactor is the same as that of the first cell in the two-cell reactor, for the same total reactor volume.

Peripherally or Subsurface-Impregnated Pellets

Reactor Lifetime. In this section we consider the case where the dimensionless inner radius of the impregnated zone $\xi_a (= r_a/R)$ is not zero. For such partially impregnated pellets, a simple, analytical expression (such as Eq. 24) for the reactor lifetime is not available. Thus, we will examine the lifetime of the reactor graphically in the $(f,h) - \xi$ plane.

We define the effective poisoning time of the i-th cell in the N-cell reactor $\tau^N_{e,i}$ to be the time required for the poison front to reach the inner radius of the impregnated zone in the i-th cell. For simplicity, the abbreviated notation $\tau_{e,i}$ will be used instead of $\tau^N_{e,i}$ unless the full notation is required for clarity. In addition, we assume that the whole reactor is filled with the same catalyst, i.e.,

$$\xi_{a,i} = \xi_{a,j} \qquad (i \neq j). \tag{35}$$

Suppose we have a plot of

$$h(\xi(\tau)) = \tau. \tag{36}$$

Then it follows from the definition of the effective poisoning time that for the first cell

$$\tau_{e,1} = h(\xi_{a,1}) \tag{37}$$

For the i-th cell ($i \geq 2$), Eq. 17 yields

$$f(\xi_{i-1}(\tau_{e,i})) = h(\xi_{a,i}(\tau_{e,i})) \tag{38}$$

which, with the aid of Eq. 35, reduces to

$$f(\xi_{i-1}(\tau_{e,i})) = h(\xi_{a,i-1}(\tau_{e,i-1})). \tag{39}$$

From the $h(\xi)$ curve defined in Eq. 36, we get

$$h(\xi_{i-1}(\tau_{e,i})) = \tau_{e,i}. \tag{40}$$

Thus, Eqs. 37, 39 and 40 constitute the operating lines of the graphical procedure which we use to determine the effective poisoning time of each cell in the reactor. Figure 6 illustrates the graphical procedure for the case of $N = 4$; $\tau_{e,i}$ in Figure 6 represents the effective poisoning time of the i-th cell.

Note that the graphical procedure used in Figure 6 involves exactly the opposite sequence to that shown in Figure 4.

Effect of Gas-Phase Mixing on Reactor Lifetime. Figure 7 illustrates the effect of the number of mixing cells on the lifetime of the reactor for the same total reactor volume. We note that $\tau^1_{e,1} < \tau^2_{e,2} < \tau^4_{e,4}$, and generally

$$\tau^N_{e,N} < \tau^M_{e,M} \text{ whenever } N > M.$$

In other words, the reactor lifetime increases with increasing number of mixing cells (i.e., with decreasing degree of gas-phase mixing). This generalization follows directly from the fact (Eq. 19) that the horizontal distance between the h-curve and the f-curve becomes larger as the poison penetration depth increases (i.e., as ξ decreases).

REACTOR CONVERSION PERFORMANCE

To illustrate the model developed here, we examine the effect of pore-mouth poisoning on the oxidation of propylene over supported Pt. H_3PO_4 is assumed to be the poison precursor.

Table 1 shows a standard set of parameter values used for the calculations. The psuedofirst-order reaction rate constant k was estimated from the specific reaction rate expression given in Oh et al. (1980), assuming the propylene concentration is low enough to ensure a large excess of oxygen and negligible inhibition of the reaction rate due to propylene chemisorption. In some of the calculations, the Thiele parameter Φ_A and the number of mixing cells

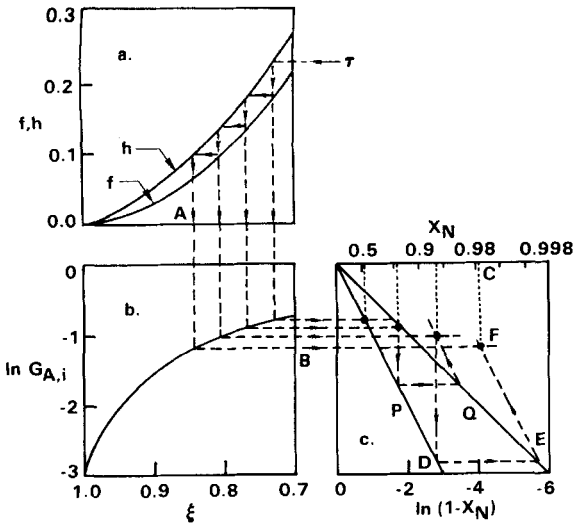

Figure 8. Graphical procedure to determine reactor conversion performance ($N = 4$, $\Phi_A = 200$).

N were perturbed from their standard values for clarity of illustration.

Reactivity of Single Pellet

The reaction rate in a single catalyst pellet is related to its effectiveness factor η which in turn is a function of the poison penetration depth and the impregnation profile.

The effectiveness factor for an isothermal spherical pellet is defined here as the ratio of the actual rate of reaction under the influence of diffusion limitation to the rate when diffusion is infinitely rapid in the volume fraction $(1 - \xi_a^3)$ of the pellet. Then the effectiveness factor for all the impregnation patterns listed in Table 2 can be obtained from Aris (1973, p. 136) with a suitable transformation of coordinates:

$$\frac{1}{\eta} = \left\{\frac{1-\xi_a^3}{y^3-\xi_a^3}\right\} \frac{1}{\eta_s(\Phi_A y, \xi_a/y)} + \frac{\Phi_A^2(1-\xi_a^3)}{3}\left\{\frac{1-y}{y} + \beta_A\right\} \tag{41}$$

where

$$\eta_s(\alpha,\sigma) = \frac{3}{\alpha^2(1-\sigma^3)}\left\{\frac{\omega + (\alpha^2\sigma - 1)\tanh\omega}{\alpha\sigma + \tanh\omega}\right\} \tag{42}$$

$$\Phi_A = R(\hat{k}S_g\rho_p/D_{e,A})^{1/2} \tag{43}$$

$$\omega = \alpha(1-\sigma) \tag{44}$$

(a) $y = \xi$, $\xi_a = 0$ for uniform impregnation,
(b) $y = \min(\xi,\xi_b)$, $\xi_a = 0$ for core impregnation,
(c) $y = \xi$ for peripheral impregnation,
(d) $y = \min(\xi,\xi_b)$ for subsurface impregnation,

and $\min(\xi,\xi_b)$ indicates the selection of the smaller between ξ and ξ_b.

Graphical Procedure to Determine Reactor's Conversion Performance

If we assume a pseudosteady-state for the gas-phase concentration of the reactant in each cell, the conversion of the main reactant can be written for an N-cell reactor as

$$x_N = 1 - \prod_{i=1}^{N} G_{Ai} \tag{45}$$

where G_{Ai}, the transfer function of the i-th cell for the reactant, is given by

$$G_{Ai} = \{1 + \eta_i(1-\epsilon)VS_g\rho_p\hat{k}/NQ\}^{-1}. \tag{46}$$

If Φ_A becomes infinitely large (i.e., in the completely diffusion-controlled regime), the transfer function for the uniformly impregnated pellet can be obtained by

$$G_{Ai} = \left\{\frac{1-(1-\beta_A)\epsilon_i}{1-(1-\beta_A)\xi_i + \mu_{Ai}\xi_i}\right\}. \tag{47}$$

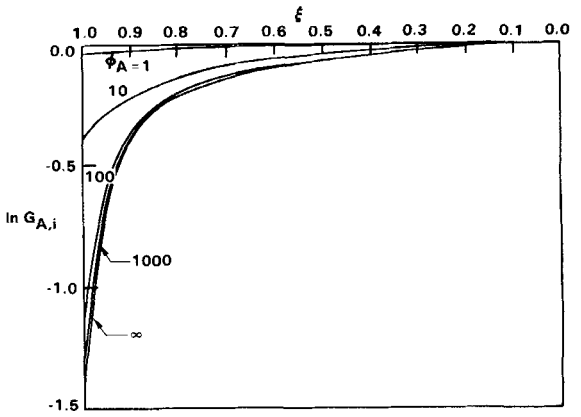

Figure 9. Effect of noble metal loading on the transfer function of the reactant.

The graphical procedure described in the previous sections can be extended to predict the conversion performance of the reactor for pore-mouth poisoning, which is illustrated in Figure 8 for the case of a first-order main reaction, a Thiele modulus of 200, and four mixing cells. The poison penetration depth at time τ in each cell can be obtained from Figure 8a, using the same procedure as was used in Figure 4; for example, point A in Figure 8a gives the radial location of the poison front for the 4th cell. The corresponding value of the transfer function for the 4th cell is given by point B in Figure 8b.

Here it may be necessary to elaborate upon how to obtain point C in Figure 8c. Suppose the conversion x_3 from the 3rd cell is known. Then the vertical line $x_N = x_3$ intersects the straight line P (with a slope of 1) at point D, and the intersection between the horizontal line passing through point D and the straight line Q (with a slope of ½) gives point E. Another straight line drawn through point E parallel to line P and the horizontal line passing through point B intersect at point F, which gives the conversion from the 4th cell at time τ. In this graphical procedure, the relation

$$ln(1-x_N) = lnG_{AN} + \sum_{i=1}^{N-1} lnG_{Ai} \tag{48}$$

has been used, which is a different form of Eq. 45.

Though the graphical procedure has been illustrated here for a first-order main reaction, it can be readily extended to the case of nonlinear kinetics with a proper modification of the transfer function diagram. However, this procedure for nonlinear kinetics would generally require some trial-and-error procedures, because the conversion and the transfer function are not separable from each other.

When the number of mixing cells is too large, the graphical procedure becomes inconvenient and inaccurate; thus, we need to solve the algebraic equations numerically. In solving Eqs. 26 and 28, the bisection method (e.g., Conte and deBoor, 1972) was found to be more effective than the Newton-Raphson iteration. While the Newton-Raphson method was too sensitive to initial guesses in some parameter ranges, the bisection method guaranteed convergence and accuracy because a unique solution for ξ is known to exist between zero and one.

Effect of Thiele Modulus

The performance of a fixed-bed reactor is directly related to the Thiele modulus Φ_A for the main reaction. The effect of the Thiele modulus on the reactor's conversion performance can be readily examined by constructing the transfer function G_{Ai} for various Φ_A values (Figure 9). In Figure 9, the Thiele modulus was perturbed by varying the noble metal loading, while the effective diffusivity

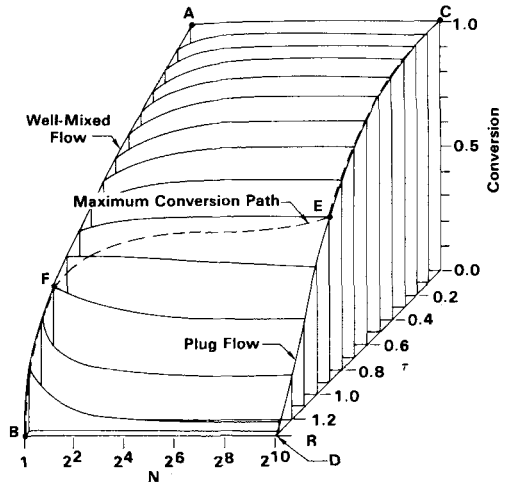

Figure 10. Effect of gas-phase mixing on the conversion at various times.

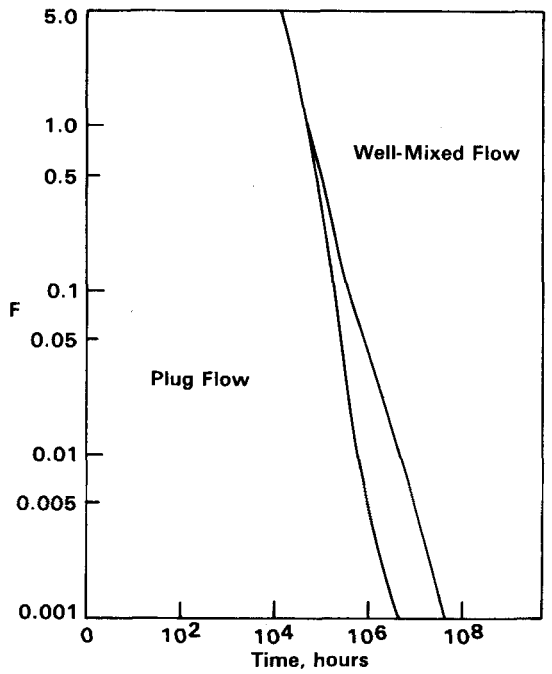

Figure 11. Effect of effective diffusivity on the transition of maximum conversion.

of the reactant was kept constant. The curve for the infinite value of Φ_A was generated using Eq. 47. It can be seen from Figure 9 that increasing the noble metal loading beyond a certain critical level provides virtually no further improvement in the conversion. This can be attributed to the fact that the process becomes increasingly influenced by diffusion as Φ_A increases. It is also interesting to note that the activity of each cell becomes less sensitive to noble metal loading as the poison penetration depth increases (i.e., as ξ decreases).

Effect of Gas-Phase Dispersion

Figure 10 illustrates the effect of the number of mixing cells (i.e., the effect of the gas-phase mixing) on the conversion performance of a catalytic converter packed with uniformly impregnated pellets under typical automobile exhaust operating conditions. (See Table 1 for the parameter values.) Though the exact plug flow condition corresponds to an infinite number of mixing cells, it was assumed in Figure 10 that 2^{10} mixing cells essentially simulate the plug flow condition.

Curves AB and CD in Figure 10 show the conversions as a function of time for a well-mixed flow condition and a "practically" plug flow condition, respectively. For $\tau < 0.9$ plug flow gives better conversion than does well-mixed flow; this trend reverses for $\tau > 1.05$. For a time period of $0.9 < \tau < 1.05$ an intermediate degree of gas-phase mixing yields the highest conversion of the main reactant (curve EF). It is well known (e.g., Levenspiel, 1972; Wei, 1975) that a plug-flow reactor gives better conversion than a well-mixed reactor when the reaction kinetics is of positive order, and the opposite is true when it is of negative order. However, when the poisoning process is coupled with the main reaction, this general rule breaks down, as demonstrated in Figure 10.

The path CEFB, the locus of maximum conversion, indicates that the optimum reactor configuration depends on the reactor operating time. That is, for a given reactor volume, a long, narrow reactor should be used when the reactor operating time is short, but a shallow reactor with a large cross-sectional area becomes more efficient for longer operating times.

It may be worth mentioning that 1,000 hours of automobile catalytic converter operation corresponds to a dimensionless time of about 0.1.

For operating conditions typical of a fully warmed-up catalytic converter (essentially isothermal operation in the turbulent flow regime), one layer of catalyst pellets amounts to one mixing cell (Wei, 1975); this translates into about 16 mixing cells for a production pellet-type catalytic converter (Table 1). Figure 10 shows that at $\tau = 0.1$ the conversion performance corresponding to $N = 16$ is essentially the same as the optimum level, indicating that the present catalytic converter has the right depth to give the best performance after 80,000 km of driving (1,000 hours of driving at 80 km/h), at least from the standpoint of catalyst poisoning by the pore-mouth mechanism.

The sharpness of the transition between E and F in Figure 10 as well as the time of its occurrence depends upon the effective diffusivities in the catalyst pellets for a given set of reactor operating conditions. This is shown in Figure 11, where the effective diffusivities of both the reactant and the poison precursor were perturbed around their standard values given in Table 1 by the same factor F. It is noted that as the effective diffusivities increase, a sharper transition of maximum conversion from the plug flow reactor to the well-mixed reactor occurs at earlier times. We can also deduce that when the factor F becomes infinitely large (i.e., in the absence of intrapellet diffusion resistances), the transition occurs right at time zero, and thus the well-mixed reactor configuration is beneficial regardless of the length of the reactor's operating time. This observation is again in contrast to the usual fixed-bed catalytic reactor behavior under non-poisoning conditions.

Design of Nondeteriorating Catalyst Pellets

In some industrial applications, it is important to maintain the reactor's conversion performance above a certain specified value at a given final time. The graphical procedure developed here can be used to design such nondeteriorating catalysts as follows.

The outer radius of the impregnation band ξ_b is determined based on the poison penetration depth at a specified final time of reactor operation. For a given ξ_b, then, the inner radius of impregnation ξ_a can be determined such that an increase in the band width does not provide further improvement in the conversion performance for a given Thiele modulus Φ_A. With this strategy of subsurface impregnation, the catalytic activity will remain constant up to the final time without experiencing deactivation due to pore-mouth poisoning.

Figure 12 illustrates how the graphical procedure in Figure 4 can be used to design a nondeteriorating catalyst.

Figure 12a shows the graphical procedure for determining the poison profile in the reactor, which was already discussed in Figure 4. In Figure 12b line B is a straight line with a slope of unity, and the vertical distance between the two lines A and B represents the sufficient impregnation band width δ, which was obtained by the following procedure. For a given value of the outer radius of the impregnation band ξ_b, the inner radius of the impregnation band ξ_a was decreased step by step, thereby increasing the impregnation

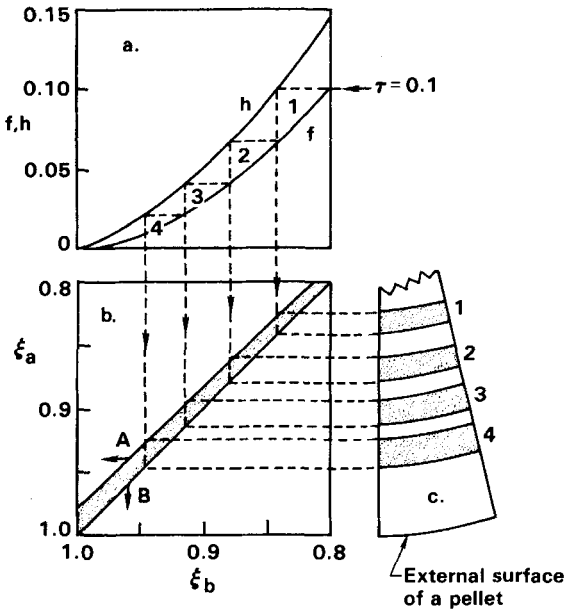

Figure 12. Subsurface impregnation for nondeteriorating catalyst pellets ($N = 4$, $\Phi_A = 200$).

band width $\xi_b - \xi_a$. The conversion performance of a mixing cell was then computed for each pair of ξ_b, ξ_a values, and the computation was terminated when the criterion

$$\Delta x_i / \Delta(\xi_b - \xi_a) \leq (10^{-7}/R)$$

was satisfied. Here $\Delta(\xi_b - \xi_a)$ is the increase in the impregnation band width, while Δx_i is the associated increase in the conversion performance of the i-th cell. The thickness of the impregnation band obtained just before the termination of the computation is defined as the sufficient band width δ for a prespecified ξ_b, in the sense that no significant improvement in the conversion performance is expected by increasing the impregnation band width beyond δ.

Figure 12c shows the location and width of the impregnation bands of the catalyst pellets in each cell. That is, it is necessary to have catalysts with different impregnation depths and band widths along the reactor length in order to operate the reactor with a constant activity under pore-mouth poisoning conditions.

NOTATION

c = concentration of the poison precursor in the intrapellet gas phase, mol/cm^3
c_A = concentration of the main reactant in the intrapellet gas phase, mol/cm^3
c_∞ = bulk gas-phase concentration of the poison precursor, mol/cm^3
$c_{\infty,A}$ = bulk gas-phase concentration of the main reactant, mol/cm^3
D_e = effective diffusivity of the poison precursor, cm^2/s
$D_{e,A}$ = effective diffusivity of the main reactant, cm^2/s
f = function defined by Eq. 7
G = cell transfer function defined by Eq. 16 or 46
h = function defined by Eq. 19
J = molar transport rate, mol/s
$\hat{k}$ = pseudofirst-order reaction rate constant of the main reaction, cm^3/(s·cm^{2}Pt)
k_m = external mass transfer coefficient, cm/s
N = total number of mixing cells in the reactor
Q = gas flow rate, cm^3/s
r = pellet radial coordinate, cm
R = radius of a pellet, cm
$\tilde{R}_A$ = rate of the main reaction per catalyst pellet, mol/s
S_g = specific active surface area of a pellet, cm^2 Pt/g pellet
t = time, s
V = total reactor volume, cm^3
V_i = volume of the i-th cell ($=V/N$), cm^3
x_i = fractional conversion by a single cell
x_N = fractional conversion by a reactor with N cells

Subscripts

a = inner radius of the impregnation band
A = main reactant
b = outer radius of the impregnation band
c = complete poison
e = effective poison
i = i-th mixing cell
o = feed condition
p = radius of the poison front
R = reference state

Greek Letters

β = inverse Biot number for mass transfer, $D_e/R\,k_m$
δ = optimal band width of subsurface impregnation
ϵ = void fraction of the reactor bed
η = effectiveness factor of a pellet
θ = dimensionless space time defined by Eq. 12
λ = saturation concentration of the poison in a pellet, mol/cm^3 pellet
μ = diffusion time to residence time ratio defined by Eq. 13
ξ = dimensionless radial position of the poison front in a pellet, r_p/R
ξ_a = dimensionless inner radius of the impregnated band, r_a/R
ξ_b = dimensionless outer radius of the impregnated band, r_b/R
ρ_p = catalyst pellet density, g/cm^3 pellet
τ = dimensionless time, $6\,D_e c_R t/R^2$
Φ_A = Thiele modulus of the main reactant defined by Eq. 43
Ψ = dimensionless concentration of the bulk gas phase, c_∞/c_R.

LITERATURE CITED

Aris, R., *The Mathematical Theory of Diffusion and Reaction in Permeable Catalysts*, **1**, Oxford University Press, London (1975).
Becker, E. R., and J. Wei, "Nonuniform Distribution of Catalysts on Supports: II. First Order Reactions with Poisoning," *J. Catal.*, **46**, 372 (1977).
Bischoff, K. B., "Accuracy of the Pseudo Steady State Approximation for Moving Boundary Diffusion Problem," *Chem. Eng. Sci.* **18**, 711 (1963).
Bischoff, K. B., "General Solution of Equations Representing Effects of Catalyst Deactivation in Fixed-Bed Reactors," *Ind. Eng. Chem. Fund.*, **8**, 665 (1969).
Carberry, J. J., and R. L. Gorring, "Time-Dependent Pore-Mouth Poisoning of Catalysts," *J. Catal.*, **5**, 529 (1966).
Conte, S. D., and C. deBoor, *Elementary Numerical Analysis*, 2nd ed., McGraw-Hill Book Co., New York (1972).
DeLancey, G. B., "An Optimal Catalyst Activation Policy for Poisoning Problems," *Chem. Eng. Sci.*, **28**, 105 (1973).
Froment, G. F., and K. B. Bischoff, "Non-Steady State Behavior of Fixed Bed Catalytic Reactors due to Catalyst Fouling," *Chem. Eng. Sci.*, **16**, 189 (1961).
Haynes, Jr., H. W., "Poisoning in Fixed Bed Reactors," *Chem. Eng. Sci.*, **25**, 1615 (1970).
Hegedus, L. L., "On the Poisoning of Porous Catalysts by an Impurity in the Feed," *Ind. Eng. Chem. Fund.*, **13**, 190 (1974).
Hegedus, L. L., and J. C. Summers, "Improving the Poison Resistance of Supported Catalysts," *J. Catal.*, **48**, 345 (1977).
Hegedus, L. L., and K. Baron, "Phosphorus Accumulation in Automotive Catalysts," *J. Catal.*, **54**, 115 (1978).
Levenspiel, O., *Chemical Reaction Engineering*, 2nd ed., John Wiley &

Sons, New York (1972).
Mecklenburg, J. C., and S. Hartland, *The Theory of Backmixing*, John Wiley & Sons, New York (1975).
Moriyama, A., "Analysis of Fluid-Solid Reaction in Fixed-Bed Reactors under Isothermal Conditions," *Trans. Iron & Steel Inst. Japan*, **11**, 176 (1971).
Murakami, Y., T. Kobayashi, T. Hattori, and M. Masuda, "Effect of Intraparticle Diffusion on Catalyst Fouling," *Ind. Eng. Chem. Fund.*, **7**, 599 (1968).
Oh, S. H., J. C. Cavendish, and L. L. Hegedus, "Mathematical Modeling of Catalytic Converter Lightoff: Single-Pellet Studies," *AIChE J.*, **26**, 935 (1980).
Olson, J. H., "Rates of Poisoning in Fixed-Bed Reactors," *Ind. Eng. Chem. Fund.*, **7**, 185 (1968).
Valdman, B., P. A. Ramachandran, and R. Hughes, "Impurity Poisoning of Catalyst Pellets," *J. Catal.*, **42**, 303 (1976).
Varghese, P., and E. E. Wolf, "Effectiveness and Deactivation of a Diluted Catalyst Pellet," *AIChE J.*, **26**, 55 (1980).
Wei, J., "Catalysis for Motor Vehicle Emissions," *Adv. in Catal.*, **24**, 57 (1975).
Wheeler, A., and A. J. Robell, "Performance of Fixed-Bed Catalytic Reactors with Poison in the Feed," *J. Catal.*, **13**, 299 (1969).

Manuscript received June 2, 1981; revision received April 21, and accepted April 30, 1982.

Hydraulic Deliquoring of Compressible Filter Cakes

Part 1: Reverse Flow in Filter Presses

Removal of liquid from filter cakes can be accomplished by mechanical or hydraulic methods after cake formation is complete. This paper deals with the latter procedure. The local porosity in porous beds (Tiller and Cooper, 1962) is a function of hydraulic pressure distribution and cake compressibility. Calculation of average porosity requires an integration of local values as determined by liquid flow patterns. As most compressions of filter cakes are irreversible, the local porosity is a function of the maximum effective pressure (frictional pressure loss) reached during cyclical operations. Reversal of flow through a cake develops radically changed pressure distributions which can be utilized to reduce local porosities. Analytical expressions are presented for reduction of average porosity brought about by reversing flow of liquid in plate-and-frame and recessed plate filter presses.

FRANK M. TILLER and LIOU-LIANG HORNG

Department of Chemical Engineering
University of Houston
Houston, TX 77004

SCOPE

Filtration engineers empirically recognize that increasing pressure results in decreases of liquid content of filter cakes. Unfortunately, highly compressible beds like colloidal silica or those arising from wastewater treatment do not respond as might be expected to direct increases in filtration pressure. Tiller and Green (1973) showed that a skin with low porosity and high flow resistance developed next to the medium during filtration of highly compressible materials. The skin deters development of frictional forces necessary to porosity reduction in a large portion of the cake. The hydraulic pressure shows little loss through much of the bed and then drops precipitously near the supporting medium. Porosity follows a similar pattern with most of the cake remaining unconsolidated while a compact layer develops where the filtrate exits.

To effect deliquoring of such cakes, the liquid flow can be reversed in direction at the end of filtration. Such reversal is a normal part of washing in plate-and-frame filter presses. When reverse flow takes place, the skin serves as a piston which compresses the unconsolidated portion of the cake. When liquid in the wash mode begins to flow, it encounters the resistant layer first. The large pressure drop across the skin is transmitted by interparticle forces throughout the cake and thereby results in substantial decrease in porosity.

Equations are developed which yield the hydraulic pressure, effective pressure, and porosity as a function of distance both for the filtration and reverse flow modes.

CONCLUSIONS AND SIGNIFICANCE

Deliquoring of filter cakes is an important operation in solid-liquid separation. Mechanical squeezing utilizing membranes in filter presses requires additional investment in equipment and direct use of hydraulic pressure as developed by pumps represents the simplest method for porosity reduction. Increase in pump pressure is the preferred method if a sufficiently dry residue can be produced. Unfortunately those highly compressible cakes which cause the most difficulty in industry are little affected by elevated pressure. For the most compressible materials, increasing pressure has negligible effect on average porosity or flow rate. Consequently, methods not dependent on elevated pressures must be utilized for deliquoring such cakes.

Reversing the direction of flow through the highly compressible bed leads to marked reduction in porosity. In filter presses, washing automatically leads to a reverse flow pattern. However, failure to recognize the effects of hydraulic, reverse flow deliquoring can negate the practical advantage in an industrial filter. If the expressed liquid is not drained but is simply dumped along with the cake into a common receiver, the aver-